Performance and interaction quality variations of a collaborative Cable-Driven Parallel Robot

Marceau Métillon, Camilo Charron, Kévin Subrin, Stéphane Caro

Performance and Interaction Quality Variations of a Collaborative Cable-Driven Parallel Robot

Marceau MÉTILLON[a], Camilo CHARRON[a], Kévin SUBRIN[a], Stéphane CARO[a,*]

[a]*Nantes Université, École Centrale Nantes, CNRS, LS2N, UMR 6004, F-44000 Nantes, France*

Abstract

In the field of large scale robotic, which is often remotely operated, having direct interaction can be disruptive for applications such as moving heavy loads or 3D printing. A Cable-Driven Parallel Robot (CDPR) is used here in physical Human-Robot Interactions (pHRI) with an admittance-based control strategy to physically interact with a user in tele-operation or in co-manipulation mode. A user experiment involving participants is designed to assess the performance of the human-robot team in a given task completion. Task performance and interaction quality metrics are defined and recorded during experiments with different robot configurations. The novelty is to provide a methodology to compare the configurations based on the performance metrics. The methodology accounts for variations of the metrics along time of use and assert a training effect leading to a progression or a regression of the performances. The experiment apparatus includes a CDPR, a user task composed of targets to reach with the robot and a handle equipped with a force sensor acting as a control input of a fixed admittance control strategy of the robot. Collected data show that the task performances and the interaction quality vary during the experiments and denote different variation profiles among the user population. Distribution of these profiles among configurations are analysed to determine the configuration that has the best training effect on users.

Keywords: Physical Human-Robot interactions, Cable Driven Parallel Robots, Performance variations, Transparency

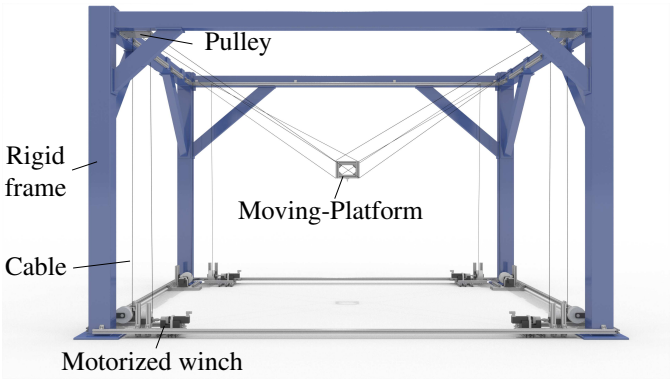

Figure 1: Main components of a CDPR

1. Introduction

A Cable Driven Parallel Robot (CDPR) belongs to a particular class of parallel robots (see fig. 1) where the Moving-Platform (MP) is linked to a base frame using cables [1]. Motors are mounted on a rigid base frame and drive winches. Cable coiled on these winches are routed through exit points located on the rigid frame to anchor points on the MP. The pose (position and orientation) of the MP is determined by controlling the cable lengths.

CDPRs have considerable advantages compared to their classical parallel robot counterparts with rigid links. Mass in motion is reduced thanks to cables being used instead of rigid limbs [2]. CDPRs provide large translation workspaces and are easier and more affordable to deploy than classical parallel robots. CDPRs are well fitted for tasks requiring a large translational workspace [3], a high payload/weight ratio [4, 5] or reconfigurability [6]. CDPRs are adapted to industrial tasks such as painting [6], intra-logistics [7] and large part printing [8].

Despite their advantages for specific tasks, CDPRs are not yet widely used in industrial environments. An obstacle to the industrial deployment of these robots is the lack of Human-CDPR Collaboration. Classical CDPRs cannot be deployed without restrictive safety measures to ensure safe working conditions for the human operator sharing the robot workspace. Non-collaborative CDPRs need large protective carter or detection systems which stop the robot when an operator is detected within the robot workspace. Such strategy prevents collision between operator and cables and/or MP but also restrain the human and the robot to work as a team in a shared workspace. A collaborative CDPR with awareness of the operator, safety measures [9, 10] and adapted control strategy would be able to work alongside the operator in a shared environment thus collaborating together on the completion of a task with a common objective. When the operator teams up with the robot, the human-robot team is able to perform tasks that neither the robot nor the human could easily perform alone [11]. The robot increases the payload capacity and the reachability of the operator and the operator brings knowledge and adaptation capacities to the team.

*Corresponding author `stephane.caro@ls2n.fr`

In order to develop such collaborative CDPRs, two main challenges need to be addressed. First an adapted control strategy allowing the operator to control the robot needs to be set-up. Then a system needs to be developed to prevent possible collisions between the operator and moving parts of the robot and ensure a safe working environment for the operator. This research addresses the first challenge, the design of a control architecture to support human-robot collaboration, and the way to measure its effectiveness. Within this context, this paper presents a methodology to measure human-robot team performance and its variation along time of use. The variation of this performance can directly assess the quality oh the human-robot interaction [12].

In addition to purely task performance metrics, interaction metrics needs to be defined to assess the quality of the human-robot teaming [13]. In the field of haptics and specifically in bilateral teleoperation, transparency is largely used to assess the quality of the human-robot interaction. The transparency is defined as the capacity of the robot to not show resistance when being actuated by the user. When the user manipulate the system, the friction and inertia present in the load and the system should not be perceptible to the user. Researches has been done toward the improvement of the transparency in teleoperation. The transparency in bilateral tele-operation is improved through friction compensation [14], use of hybrid control algorithm and passive and active actuators combination [15] or the use of series elastic actuation in [16]. A novel multidimensional transparency is defined in [17] which dimensions are perceptual, local motor and remote motor transparency. When the system used is in a co-manipulation meaning that the user is physically interacting on an interaction port located on the robot end-effector various strategies are studied to increase the transparency. Human motion prediction allows a collaborative robotic system to increase transparency [18]. The user hand impedance compensation reduce the effort required to move the system thus improving the transparency [19]. Generally, the transparency improvement sought is evaluated as a subjective value assessed by users when comparing different control algorithms and robot configurations. To the best of the author knowledge, there is no transparency metric generally used to study and compare both teleoperation and co-manipulation cases. In addition, there is no study on the variation of the transparency and a training effect during the completion of a task. When a human performs a repeated task win co-manipulation with a robot, the team performance may vary for at least two reasons. The first reason deals with the task characteristic itself. Some parts of the task may be substantially more difficult than others to perform. For example, the effort needed to reach the same criterion of speed or precision on two different parts of the task may be different for the user. The second reason concerns the human adaptation [20]. The experience may induce internal modification of the user which in turns modifies the human behaviour. The human may learn from the CDPR behaviour then modify his behaviour in order to maximize one or several team performance criteria. The human may change his/her satisfying performance criterion in order to maintain a good situation mastery [21].

This paper presents a methodology, which permits to measure and analyse human-robot team performance and their variations. Since there are human inter-individual differences in adaptation and development [22], the methodology is constructed in order to allow the analysis of the team performance with any human using the CDPR [23]. The collected performance measures are objective and do not rely on survey or operator assessment [24]. In the scope of this paper, the usability of a CDPR is studied. Among the dimensions of usability this paper studies the human performance and training effect of CDPRs [25, 26]. Furthermore, the presented methodology allows to compare different configurations of robot and is also applicable to compare teleoperation and co-manipulation working modes. The task influence on the performance can be assessed for each case. The training effect is analysed and classified in profiles. The profile distribution is compared over configurations to give insights on the one that have a maximum of user improving performance thanks to the training effect.

The remaining sections are organized as follows: Section 2 presents the user experiment methodology. Section 3 provides the robot modelling and the control algorithm used in the experiment. Section 4 details the user experiment performed to apply the methodology. Section 5 presents the results analysis. Section 6 gives a discussion. Finally, Section 7 draws conclusions and present perspectives.

2. User experiment methodology

In this section the methodology of the performance analysis is detailed. The apparatus and the user task used to apply the methodology are also presented.

The method relies on performance criteria based on the considered task and the human-robot team performance. It is possible to compare the performance criteria and their variation along time for each user of the system during an experiment. The performance criteria are to be used and compared between different set of experiments where the mechanical configuration of the CDPR changes. Separate experimentation cases are defined where the task and the control scheme remain the same but the CDPR mechanical configuration changes. This approach would highlight a tangible effect of the configuration on the team performance. It is worth noting that the control scheme of the robot is not adaptative. The control parameters are set once and for all configurations which means that a variation of performance along an experiment is only attributable to human behaviour.

2.1. Use Cases

The mechanical configuration of a CDPR includes the number and arrangement of cables as well as the position of anchor and exit points. The configuration has a direct impact on the Degrees of Freedom of the end-effector and the size of the workspace reachable by the MP. One aspect of the performance variation evaluation method is to study the impact of the configuration on the performance. Two different mechanical configuration cases are defined to be studied using the method and are presented in Fig. 2:

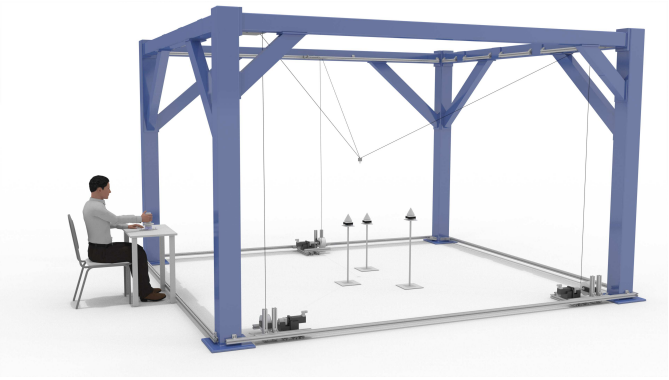

(a) First Use Case (UC1) - Teleoperation of a platform with three cables

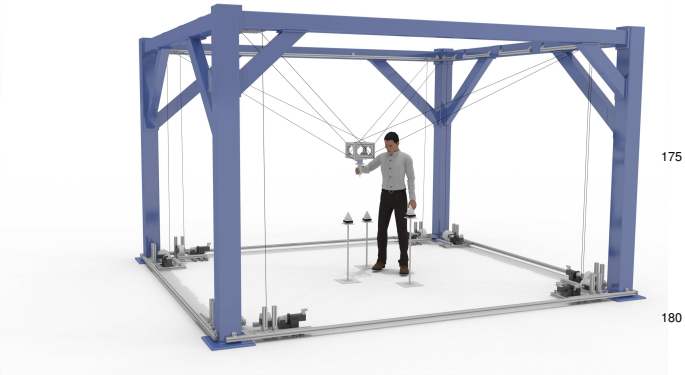

(b) Second Use Case - (UC2) - Co-manipulation of a platform with eight cables

Figure 2: The two Use Cases (UC1 and UC2) considered

- The first Use Case (UC1) includes a CDPR with three cables and a MP ($40 \times 40 \times 60$ mm) considered as a point-mass as the cables are attached to the same anchor point on the MP as shown in Fig. 2a. Using three cables, this MP is doted of 3 Degrees of Freedom and can only describe translational motions and it is not possible to control the rotation of the end-effector. In this Use Case, the MP is used in teleoperation, the user is seated outside of the robot workspace and operates the robot remotely. The distance between the user and the centre point of the task workspace is 2.7 m.

- The second Use Case (UC2) features a CDPR with eight cables and a bigger MP ($280 \times 280 \times 200$ mm) which has a parallelepiped shape as shown in Fig. 2b. With eight cables it is possible to translate and orientate the end-effector of the robot. In addition, in this case, the robot is in a direct pHRI co-manipulation mode. The user shares the robot and task workspace, being seated next to the task, at a distance of 0.45 m of the task workspace centre point.

2.2. *Apparatus*

In both UCs the CRAFT CDPR prototype, shown in fig. 3 and located in LS2N, Nantes, France is used. Its size is 3.75 m x 4.34 m x 2.78 m. The prototype is equipped with eight motorized winches and cables. Reconfigurable pulleys enable

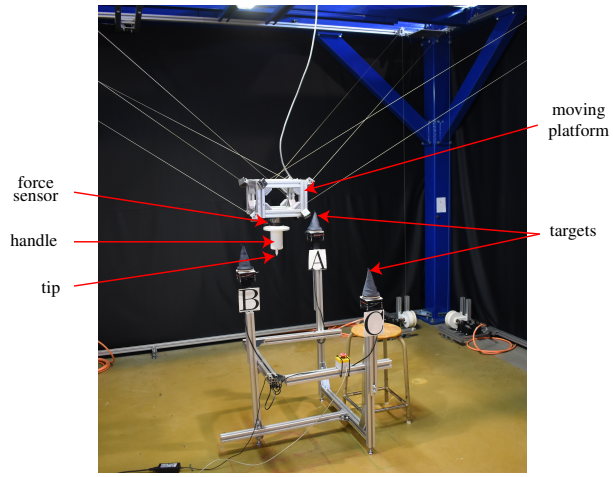

Figure 3: User experiment setup

the reconfigurability of the robot and allow the implementation of the two UCs.

A 3D printed white cone which tip is pointing toward the ground is attached to the MP and act as the end-effector of the robot. A structure holding three air inflated fabric cones is set in the middle of the robot workspace. The fabric is inflated by electric fans so that the cone tips are pointing toward the ceiling of the structure. The tip of each cone represents a target respectively named A, B and C.

The participant task is to align the tip of the end-effector with the tip of three targets successively. Six paths are defined as straight line segments between the three points A, B and C. Those paths are denoted as AB, BC, CA, AC, CB and BA. The definition of this task was inspired by Piaget's research on the spatial field and the elaboration of groups of displacements in the child. This task was designed in order to compare each displacement (eg. A to B) with its inverse (eg. B to A) and to check the associative property of the displacements. [27] The air inflated cone tips representing the targets give a physical landmark on the position of the target while ensuring the robot does not notably interact physically with the target. In the context of this work, only the pHRI is studied and not the physical interactions between the robot and its environment. In addition to the robot and its controller, the cell is equipped with a computer collecting data and measurements from the robot controller during the experiment. A camera records the participant hand acting on the handle while a second camera records the end-effector motion throughout the robot workspace. The computer hosts a task monitoring routine which watches the participant performance and delivers corresponding audio instructions to the participant.

3. Robot modelling and control

In this section, the modelling and control algorithm of the CDPR used in the experiment are detailed. The Inverse Geometric Model (IGM), Inverse Kinematic Model (IKM) and the dynamic models are expressed and used in the detailed control

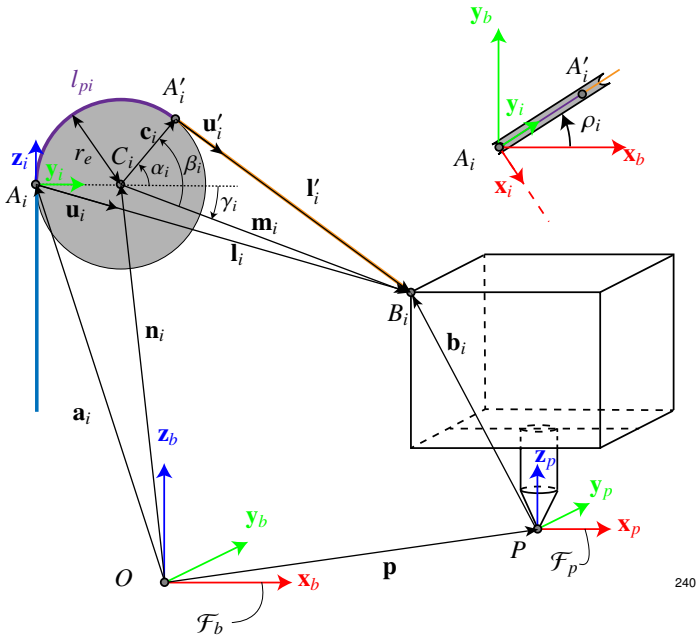

Figure 4: i-th loop closure considering pulley model

strategy. The admittance-based control law for pHRI with the CDPR is described as well.

3.1. Inverse Geometric Model (IGM)

Figure 4 shows the i-th loop closure and geometric parameters of the CDPR. A base frame $\mathcal{F}_b = (O, \mathbf{x_b}, \mathbf{y_b}, \mathbf{z_b})$ is attached to the robot base. The MP frame is denoted as $\mathcal{F}_p = (P, \mathbf{x}_p, \mathbf{y}_p, \mathbf{z}_p)$. Exit points A_i are located on the exit pulleys on the rigid frame though which cables are routed from the motorized winches. Anchor points B_i are the points located on the MP where cables are attached. A unit vector $\mathbf{u}_i$ expresses the direction of the cable between the exit points and the anchor points. Thus the loop closure equation associated to each cable is expressed as:

$$ {}^b\mathbf{l}_i = l_i {}^b\mathbf{u}_i = {}^b\overrightarrow{A_iB_i} = {}^b\mathbf{R}_p {}^p\mathbf{b}_i + {}^b\mathbf{p} - {}^b\mathbf{a}_i = {}^b\mathbf{b}_i + {}^b\mathbf{p} - {}^b\mathbf{a}_i \quad (1) $$

with $i \in [\![1, \ldots, m]\!]$, m being the cable number. ${}^b\mathbf{l}_i$ is the i-th cable vector, ${}^b\mathbf{a}_i$ is the exit point coordinate vector corresponding to the point A_i as expressed in the frame $\mathcal{F}_b$, ${}^p\mathbf{b}_i$ is the coordinate vector of anchor point B_i as expressed in the frame $\mathcal{F}_p$, ${}^b\mathbf{p}$ is the vector going from O to P expressed in the frame $\mathcal{F}_b$ and ${}^b\mathbf{R}_p$ is the rotation matrix between $\mathcal{F}_b$ and $\mathcal{F}_p$.

We can then write the i-th unit cable vector:

$$ {}^b\mathbf{u}_i = \frac{{}^b\mathbf{l}_i}{l_i} \quad (2) $$

with l_i being the i-th cable length so that $l_i = \|\mathbf{l}_i\|_2$.

In the geometric model, it is necessary to take into account the pulley model. Indeed, using two axis pulleys implies to have moving exit-point when the MP moves. The pulley model accounts for the displacement of the pulley and correct the desired cable length accordingly. The figure 5 shows the main

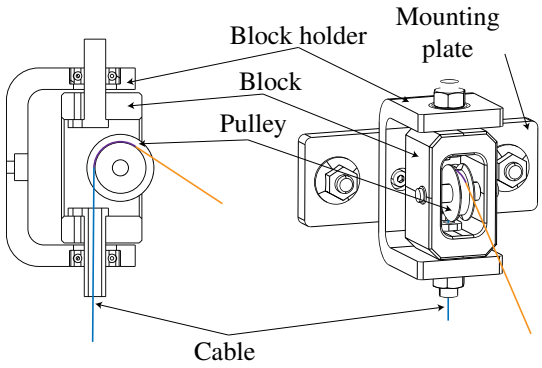

Figure 5: Two axis pulley

components of the pulleys routing the cables. The pulleys are composed of a block holder which is rigidly attached to the robot frame. A block is on a vertical axis revolute joint with the block holder. A pulley mounted on ball-bearing is linked through an horizontal axis revolute joint with the block. The cable enters the block through a bored hole on the vertical revolute axis and is wrapped around the pulley before exiting the pulley and being attached to the MP.

A frame $\mathcal{F}_i$ is attached on the i-th pulley with A_i as origin and $\mathbf{x}_i$, $\mathbf{y}_i$ and $\mathbf{z}_i$ as axis. The axis $\mathbf{z}_i$ is vertical and the axis $\mathbf{y}_i$ goes through the point A_i and the pulley centre C_i. Cable core is contained in the plane defined by vectors $\mathbf{y}_i$ and $\mathbf{z}_i$. The angle describing the rotation of the block is denoted ρ_i and is obtained as:

$$ \rho_i = \text{atan2}\left(l_{yi}, l_{xi}\right) \quad (3) $$

where l_{yi} and l_{xi} are the component of $\mathbf{l}_i$ along the axis $\mathbf{x}_b$ and $\mathbf{y}_b$ respectively as expressed in the frame $\mathcal{F}_b$.

Vector ${}^b\mathbf{n}_i$ goes from the base frame origin to the pulley centre C_i and is expressed as:

$$ {}^b\mathbf{n}_i = {}^b\mathbf{a}_i + r_e {}^b\mathbf{R}_i \, \mathbf{y}_b = {}^b\mathbf{a}_i + r_e {}^b\mathbf{y}_i \quad (4) $$

with r_e the winding radius of the cable core on the pulley and ${}^b\mathbf{R}_i$ the rotation matrix between the frame $\mathcal{F}_b$ and $\mathcal{F}_i$ so that:

$$ {}^b\mathbf{R}_i = \mathbf{R}_{\mathbf{z}i}(\rho_i - \pi/2) = \begin{bmatrix} \cos(\rho_i - \pi/2) & -\sin(\rho_i - \pi/2) & 0 \\ \sin(\rho_i - \pi/2) & \cos(\rho_i - \pi/2) & 0 \\ 0 & 0 & 1 \end{bmatrix} \quad (5) $$

Vector ${}^b\mathbf{m}_i$ goes from the pulley centre C_i to the anchor point B_i:

$$ {}^b\mathbf{m}_i = {}^b\mathbf{b}_i - {}^b\mathbf{n}_i \quad (6) $$

The vector going from the pulley centre point C_i, to exit point on the pulley groove A'_i is denoted as $\mathbf{c}_i$. Vector ${}^b\mathbf{c}_i$ is expressed in the base frame $\mathcal{F}_b$ as:

$$ {}^b\mathbf{c}_i = r_e \begin{bmatrix} \cos(\rho_i)\cos(\alpha_i) \\ \sin(\rho_i)\cos(\alpha_i) \\ \sin(\alpha_i) \end{bmatrix} \quad (7) $$

with

$$\alpha_i = \beta_i + \gamma_i \tag{8}$$

and

$$\beta_i = \text{atan2}(l'_i, r_e) \tag{9}$$

and

$$\gamma_i = -\arcsin\left(\frac{({}^b\mathbf{a}_i - {}^b\mathbf{b}_i)^T\ {}^b\mathbf{z}_i}{\|\mathbf{m}_i\|_2}\right) \tag{10}$$

The i-th cable vector, from exit point on pulley A'_i and the anchor point:

$${}^b\mathbf{l}'_i = {}^b\mathbf{m}_i - {}^b\mathbf{c}_i \tag{11}$$

The unwind cable length between point A'_i and anchor point B_i:

$$l'_i = \sqrt{\mathbf{m}_i\,\mathbf{m}_i^T - r_e^2} \tag{12}$$

and the unit vector ${}^b\mathbf{u}'_i$

$${}^b\mathbf{u}'_i = \frac{\mathbf{l}'_i}{l'_i} \tag{13}$$

The total cable length between entry point on the pulley, A_i, and anchor point on the MP, B_i, is expressed as:

$$l_{fi} = l'_i + l_{pi} \tag{14}$$

where l_{pi} is the cable length that is wind around the pulley so that:

$$l_{pi} = r_p(\pi - \alpha_i) \tag{15}$$

with r_p is the winding radius of the cable core around the pulley.

The corresponding joint position is obtained given the cable length l_{fi} and the winch radius r_w as:

$$\mathbf{q} = \frac{\mathbf{l}_f}{r_w} \tag{16}$$

3.2. Inverse Kinematic Model (IKM)

The desired cable velocity vector $\dot{\mathbf{l}}_d$ is obtained using the Forward Jacobian matrix $\mathbf{A}$ as:

$$\mathbf{A}\mathbf{t}_d = \dot{\mathbf{l}}_d \tag{17}$$

where $\mathbf{t}_d = [\mathbf{v}_d\ \boldsymbol{\omega}_d]^\intercal$ is the twist of the MP with $\mathbf{v}_d$ being the desired translational velocity and $\boldsymbol{\omega}_d$ being the desired angular velocity of the MP.

$$\mathbf{A} = \begin{bmatrix} {}^b\mathbf{u}'_1 & {}^b\mathbf{b}_1 \times {}^b\mathbf{u}'_1 \\ \vdots & \vdots \\ {}^b\mathbf{u}'_i & {}^b\mathbf{b}_i \times {}^b\mathbf{u}'_i \\ \vdots & \vdots \\ {}^b\mathbf{u}'_m & {}^b\mathbf{b}_m \times {}^b\mathbf{u}'_m \end{bmatrix}_{6\times m} \tag{18}$$

The desired actuator velocity vector $\dot{\mathbf{q}}_d$ is obtained using the cable velocity $\dot{\mathbf{l}}_d$ and the winch radius r_w as:

$$\dot{\mathbf{q}}_d = \frac{\dot{\mathbf{l}}_d}{r_w} \tag{19}$$

3.3. Dynamic model

The dynamic equilibrium of the MP is written as [28]:

$$\mathbf{W}\boldsymbol{\tau} - \mathbb{I}_p\dot{\mathbf{t}}_d - \mathbf{C}\mathbf{t}_d + \mathbf{w}_h + \mathbf{w}_g = \mathbf{0}_m \tag{20}$$

with $\boldsymbol{\tau}$ being the cable tension vector, $\mathbb{I}_p\dot{\mathbf{t}}_d$ is the dynamic effect wrench with $\mathbb{I}_p$ being the spatial inertia matrix of the MP and $\dot{\mathbf{t}}_d = [\dot{\mathbf{v}}_d\ \dot{\boldsymbol{\omega}}_d]^\intercal$ is the desired acceleration vector of the MP, $\mathbf{w}_h = [\mathbf{f}_h\ \mathbf{m}_h]^\intercal$ is the external wrench applied by the user to the MP containing force and moment, $\mathbf{w}_g$ is the wrench due to the gravity force, $\mathbf{C}\mathbf{t}_d$ is the term of the centrifugal and Coriolis wrenches and $\mathbf{W}$ is the pose-dependent wrench matrix associated to the MP taking the form:

$$\mathbf{W} = \begin{bmatrix} {}^b\mathbf{u}_1 & \dots & {}^b\mathbf{u}_i & \dots & {}^b\mathbf{u}_m \\ {}^b\mathbf{b}_1 \times {}^b\mathbf{u}_1 & \dots & {}^b\mathbf{b}_i \times {}^b\mathbf{u}_i & \dots & {}^b\mathbf{b}_m \times {}^b\mathbf{u}_m \end{bmatrix}_{6\times m} \tag{21}$$

3.4. Control architecture

3.4.1. Admittance

The robot control interface consists into a 3D printed handle mounted on a three-axis force and torque sensor. In the UC1, the robot is controlled in teleoperation as shown in Fig. 2a. The control interface is rigidly fixed on the table located outside the robot so that the participants have the handle in front of them and can see the MP within the robot workspace. In the UC2, the interface is mounted on the bottom frame of the MP, as depicted in Fig. 2b. The force sensor measures the force $\mathbf{f}_h$ exerted by the hand of the participant on the handle. An admittance control law converts the measured force into a desired translational acceleration of the MP using an admittance control that was derived from [29]:

$$\dot{\mathbf{v}}_d = \frac{\mathbf{f}_h - \mathbf{f}_v}{m_v} \tag{22}$$

m_v is a virtual mass used to provide the user with an inertial feeling of the MP and $\mathbf{f}_v$ is a virtual force defined as:

$$\mathbf{f}_v = \begin{cases} k_v\ \text{sign}\,(\mathbf{v}_d) & \text{if} \quad \mathbf{v}_d \neq 0 \\ k_v\ \text{sign}\,(\mathbf{f}_h) & \text{if} \quad |\mathbf{f}_h| \geq f_t \text{ and } \mathbf{v}_d = 0 \\ \mathbf{f}_h & \text{if} \quad |\mathbf{f}_h| < f_t \text{ and } \mathbf{v}_d = 0 \end{cases} \tag{23}$$

with f_t a force threshold used to yield the admittance control robust with regard to force sensor drift. k_v is a dissipative term that will let the MP decelerate and stop if the user does not apply any force to the handle.

Given the desired acceleration computed using the admittance law, the desired speed and position of the MP are obtained using a first and second order integral of the acceleration respectively:

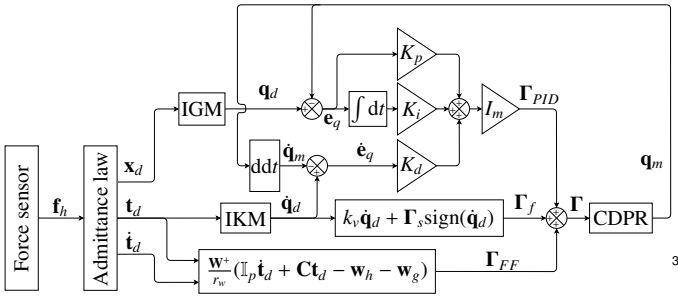

Figure 6: Admittance control scheme for HRI

$$\mathbf{v}_d = \int \dot{\mathbf{v}}_d \, dt \tag{24}$$

$$\mathbf{p}_d = \int \mathbf{v}_d \, dt = \iint \dot{\mathbf{v}}_d \, dt^2 \tag{25}$$

In addition to the definition of the desired translational acceleration, velocity and position, the admittance control also virtual limits on accelerations so that the robot does not let the participant reach the limits of the task workspace which is a subspace of the manipulator workspace. The manipulator workspace associated to UC1 is smaller than the one associated to UC2. Thus, the task is conveniently located in the robot cell so that in both configurations, the MP can reach all of the task workspace. A function routine checks the position of the MP and sets a force opposed to the human force so that the MP decelerates and never crosses the task workspace limits.

The MP pose describes the MP position and orientation expressed in the base frame $\mathcal{F}_b$. The desired MP pose is denoted is expressed as $\mathbf{x}_d = [\mathbf{p}_d \, \mathbf{r}_d]^\mathsf{T}$ $\mathbf{p}_d$ and $\mathbf{r}_d$ being the desired the point-displacement and orientation vectors of the MP, respectively. The Euler parameters are used to parametrize the MP orientation. In UC1, the MP can be considered as a point-mass to which the three cables are connected. As a consequence, in order to compare the performances obtained with the two use cases, only the the three degrees of freedom translational motions of the MP are controlled. Therefore, the orientation of the MP is kept constant in UC2. Note that the rotational motions of the MP are constrained with the control system in UC2, and not geometrically. It means that for both UC1 and UC2, the admittance law only controls the translational motion of the MP, that is to say translational acceleration $\dot{\mathbf{v}}_d$, velocity $\mathbf{v}_d$ and position $\mathbf{p}_d$. In UC2, the MP orientation is kept null by the control system.

3.4.2. Control scheme

The control scheme of the robot in the UC2 is shown in Fig. 6. The desired trajectory in the operational workspace is obtained using the admittance law described in equation (23). A desired MP pose $\mathbf{x}_d$, twist $\mathbf{t}_d$ and acceleration $\dot{\mathbf{t}}_d$ are obtained as a function of the force exerted by the user on the handle $\mathbf{f}_h$. Using the IGM of the robot, the desired joint position $\mathbf{q}_d$ is computed. The desired joint velocity $\dot{\mathbf{q}}_d$ is obtained using the IKM of the robot.

A Proportional-Integral-Derivative controller issues a correction torque Γ_{PID} using the measurement of the joint position error $\mathbf{e}$, the time-derivative of the joint error $\dot{\mathbf{e}}_q$ and the integral of the joint error $\int \mathbf{e}_q \, dt$ such as:

$$\Gamma_{PID} = I_m \left(K_p \, \mathbf{e}_q + K_i \int \mathbf{e}_q \, dt + K_d \, \dot{\mathbf{e}}_q \right) \tag{26}$$

where I_m is the motor and gearbox inertia, K_p is the proportional correction gain, K_i is the integral correction gain and K_d is the derivative correction gain.

A term anticipating the motor and gearbox friction $\mathbf{\Gamma}_f$ is computed using a Coulomb and viscous friction model denoted as:

$$\mathbf{\Gamma}_f = k_v \, \dot{\mathbf{q}}_d + \mathbf{\Gamma}_s \, \text{sign}(\dot{\mathbf{q}}_d) \tag{27}$$

where k_v is the viscous friction coefficient and $\mathbf{\Gamma}_s$ is the static friction torque. The feed forward term of the torque $\mathbf{\Gamma}_{FF}$ is computed to anticipate the torque needed to fulfil the static and dynamic equilibrium of the MP as:

$$\mathbf{\Gamma}_{FF} = \frac{\mathbf{W}^+}{r_w} \left(\mathbb{I}_p \, \dot{\mathbf{t}}_d + \mathbf{C} \, \mathbf{t}_d - \mathbf{w}_h - \mathbf{w}_g \right) \tag{28}$$

$\mathbf{W}^+$ being the pseudo-inverse of the wrench matrix. The control torque exerted by the motors on the winches is computed as the sum of the feed-forward, the friction anticipation and the correction torques as:

$$\mathbf{\Gamma} = \mathbf{\Gamma}_f + \mathbf{\Gamma}_{FF} + \mathbf{\Gamma}_{PID} \tag{29}$$

4. Human-robot team experiment

4.1. Participants

The study involved 49 participants, 30 participants for UC1 and 19 participants for UC2. In the UC1, the ages are between 18 and 62 years with a mean of 37.17 years and a standard deviation of 12.45 years. In the UC2, the ages of the participants are between 20 and 49 years with a mean of 28.37 years and a standard deviation of 8.19 years. Most of the participants are recruited from the staff of École Centrale de Nantes. The participants were adult with a normal or corrected to normal vision. All participants are required not to have ever taken part to this experiment or a precedent stage of this experiment before. This condition ensures that they have no experience and allows to study the training effect of the considered robot. They signed a written informed consent in order to take part in the experiment[1].

4.2. Procedure

The experimentation includes two manipulation phases where each participant manipulates the robot. The first one consists in a familiarization phase while the second is the user task experimentation.

[1]The experimental protocol was approved by the University of Nantes ethical committee.

4.2.1. Familiarization phase

The familiarization aims to ensure that each participant understands how the robot behaves when he/she acts on the handle. Before the familiarization phase, the operating of the robot is orally explained to the participant. The MP would place itself in a zone of the robot workspace free of any object where no collision between cables and environment or between MP and environment can occur. Then the participant is asked to perform simple movements with the robot such as moving the platform to the left and to the right, to the top and to the bottom and to the background and to the foreground.

4.2.2. Experimentation phase

The experimentation phase aims to measure the human-robot team performance variations. Once the participant has understood how to operate the robot the user task is orally explained. The participant is asked to perform as much as possible paths during the time of the experiment (10 minutes). The paths should be as close as possible to straight line between the targets. An audible signal informs the participant that the experiment started then a speech synthesizer gives the instruction as to which target the user should aim. When the required target is reached, the synthesizer issues the next target to reach. If the participant has not reached a target in a given amount of time, a routine repeats the last instruction to the participant. An audible signal lets the participant know when the experiment comes to an end. A video displaying an extract of one participant of each UC can be found using this link [2].

4.3. Data collection

During the robot use, all the variables defined in the control scheme of the robot are computed in real-time with a control frequency $f_s = 1$ kHz. A computer communicates with the robot and collects the data of the control scheme in real-time to record it in a file. For each participant of each UC, the variables such as desired MP pose, cable length and velocities, joint position and velocities are recorded accordingly with the running time of the task. Data from the robot sensors (i.e. the force sensor mounted on the handle and the joint position encoders) are also collected and recorded with the same time scale. Figure 7 shows the data collected during the task execution for participant #10 in UC2. Figure 7a plots the force exerted by the user on the handle. Figure 7b plots the recorded MP pose.

Using the data collected during the experiment, additional variables are computed for each sampling time. The variable time, deviation and transparency will be used to compute dependant variables for the forthcoming performance analysis.

4.3.1. Time

A timer runs from the beginning to the end of the experiment and records the task progression along time. The current time when targets are reached is saved in a variable.

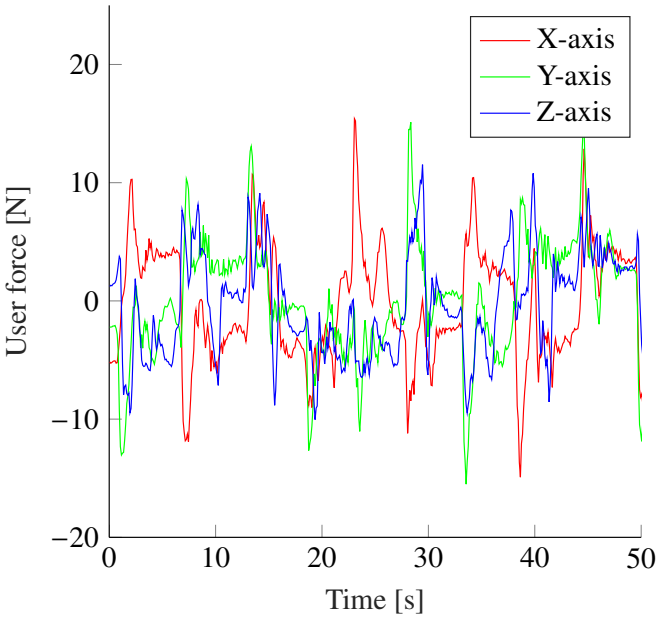

(a) Force as measured by the force sensor during experiment

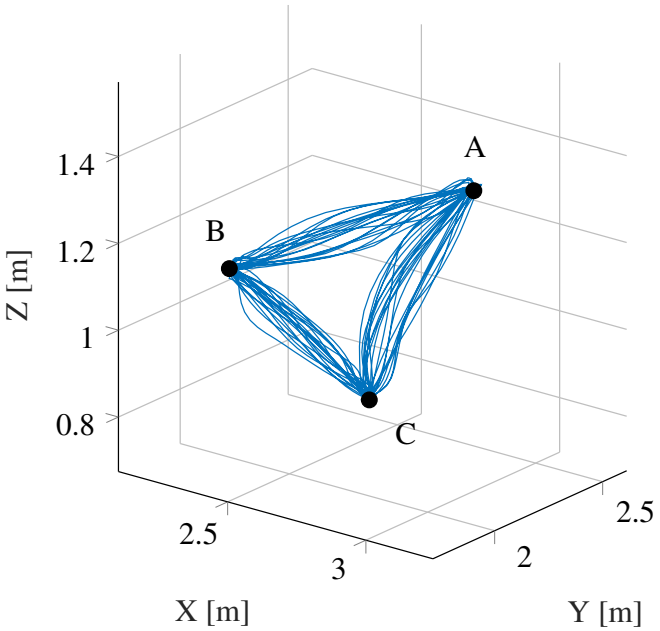

(b) Path followed by the Moving Platform during experiment

Figure 7: Data collected during the experimentation in UC2 for participant #10

[2] www.metillon.net/mechatronics_video

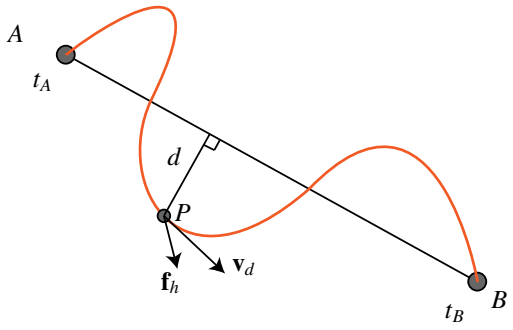

Figure 8: Ideal path (black), end-effector tip path during user experiment (orange)

4.3.2. Deviation

An ideal path is defined as a straight lines between targets. The deviation is the distance from the tip end-effector to the ideal path. This variable is a scalar that must have a low value to indicate a good performance in terms of precision of the user in the task completion.

4.3.3. Transparency

The transparency describes the collinearity of the force exerted by the user on the handle and the MP velocity. For the sake of clarity and without loss of generality, only the translational movements of the MP are considered in this paper. Therefore, the transparency of the CDPR used as a human-robot interface is defined as follows:

$$\mu = \mathbf{v}_n^{\mathsf{T}} \, \mathbf{f}_{hn} \tag{30}$$

where $\mathbf{v}_n$ and $\mathbf{f}_{hn}$ are the unit vectors of $\mathbf{v}$ and $\mathbf{f}_h$, respectively. The transparency describes the collinearity of the velocity of the MP with the force applied by the operator. The direction of the force applied by the human, defines the desired direction of motion. μ ranges from -1 to 1 where -1 indicates opposite direction of the user force and the displacement direction of the MP. 0 indicates the orthogonality between the user force and the MP displacement direction while 1 indicates a perfect collinearity that means the MP moves in the direction sought by the user. As this indicator spans the range -1 and 1, averaging the transparency would lead to bias in interpretation around a null average. Therefore an additional index ν is defined so that:

$$\nu = 1 - \mu \tag{31}$$

where ν spans over $[0, 2]$. The lower bound, 0, denotes a good transparency as force and velocity are collinear. The 1 value indicates orthogonality and 2 indicates an opposite direction of motion with the user force direction. ν does not suffer from the bias induced by the averaging. Figure 8 details the geometric entities associated to the computed deviation and transparency.

4.4. Data aggregation

At the beginning of the experimentation, the supervisor asks the participant to reach the first target (A). When the user reaches the requested target, the data collection starts and the supervisor requests the user to reach the following target (B). During the data collection, the supervisor keeps track of the task state and records the current path in a variable according to the time. The task state is used afterhand to cut the collected dataset in sequence of data for each path performed by the user.

4.5. Dependent variables

Using the data sequences, dependent variables, known as performance criteria for the deviation and completion time and interaction quality index for transparency are computed.

Time. The *Time* variable times the completion of each path. This index accounts for the different lengths of the segments being weighted by a distance ratio.

Deviation. The *Deviation* index represents the mean of the deviation over the path sequence.

Transparency. The *Transparency* response is the mean of the transparency index ν over the path sequence.

4.6. Independent variables

Two independent variables are identified to explain the performance variation. The two variables PerformedPath and PathType denote the effect of training and task influence respectively.

PerformedPath. PerformedPath is a counter of the number of path completed by the user during the experiment. It starts at 0 and is incremented of 1 every time a path is completed.

PathType. The PathType determines which path the user is completing and if the task has an effect on the performance. It is a categorical variable that has six levels corresponding to all paths determined by targets A, B and C that are denoted PathType_AB, PathType_BA, PathType_AC, PathType_CA, PathType_BC and PathType_CA.

5. Performance analysis

5.1. Analysing the task and UC effect on the human-robot performances

In addition to the effect of the UC on the performance, it is necessary to determine if the task itself has an influence on the performance. As the paths composing the task are not equivalent in term of distance and arrangement in the robot workspace, such difference can lead to a variation of the performance.

To identify such influence, a global analysis of variance (ANOVA) was led using all the observations of PerformedPath of all the users of both UCs (3106 observations). A model including the UC, the PathType and the UC:PathType interaction was defined to highlight any effect of the PathType on overall performance but also the interaction of UC and PathType which would indicate a varying effect of the nature of the task among the Use Cases. An ANOVA analysis was performed for each response, *Time*, *Deviation* and *Transparency*.

Table 1: Summary of ANOVA for *Deviation*, *Time* and *Transparency*, ** denotes a p-value inferior to 0.01, * denotes a p-value between 0.01 and 0.05 and n.s. indicates a p-value superior to 0.05

Performance	Factor	η^2	F value	df
Time	UC	0.3108	1445.882 **	1
	PathType	0.0176	16.386 **	5
	UC:PathType	0.0043	4.015 *	5
Deviation	UC	0.2488	1055.833 **	1
	PathType	0.0189	16.041 **	5
	UC:PathType	0.0017	1.475 n.s.	5
Transparency	UC	0.2908	1294.519 **	1
	PathType	0.0094	8.354 **	5
	UC:PathType	0.0025	2.231 *	5

Table 2: Overall performance of UCs

	Time [s]		Deviation [mm]		Transparency [-]	
	Mean	SD	Mean	SD	Mean	SD
UC1	18.04	5.47	74.48	26.23	0.60	0.08
UC2	8.91	3.19	28.31	11.04	0.77	0.12

Table 1 summarizes the ANOVA for each response, the results indicate a significance of the UC and PathType coefficient for all three responses ($p << 0.05$) and a significance for the UC:PathType coefficient for *Time* and *Transparency*. However, when studying the correlation ratio η^2 of the predictor, it can be noted that PathType and UC:PathType effect on three responses is very small ($\eta^2 < 0.02$). These values indicate that these predictors represent less than 2% of the variability of the responses thus denoting that the PathType is not influencing the performances. It is possible to conclude that the nature of the task has a negligible effect on the human-robot team performances.

Table 2 details the average and the standard deviation of performance criteria of both UCs. It can be seen that the mean value of *Time* for UC1 is 18.04 s (SD = 5.47 s) and for UC2 is 8.91 s (SD = 3.19 s). For the *Deviation* variable, the mean is 74.48 mm (SD = 26.23 mm) for UC1 and 28.31 mm (SD = 11.04 mm) for UC2. In term of *Transparency*, the mean value is 0.60 (SD = 0.08) for UC1 and 0.77 (SD = 0.12) for UC2. The UC2 presents a better performance in term of the task performance. However in term of interaction quality, the mean transparency index of UC2 is bigger than the UC1 value denoting a worse transparency in UC2 than in UC1.

5.2. Analysing the relationships between performance criteria

In order to compare the average performance of each participant of both UCs, the mean value of each performance criteria is computed for each participant. Figure 9 plots the mean value of each performance per participant. It can be seen that the variability in term of *Time* and *Deviation* performance is more important in UC1 than in UC2. The *Transparency* has more variability in the UC2.

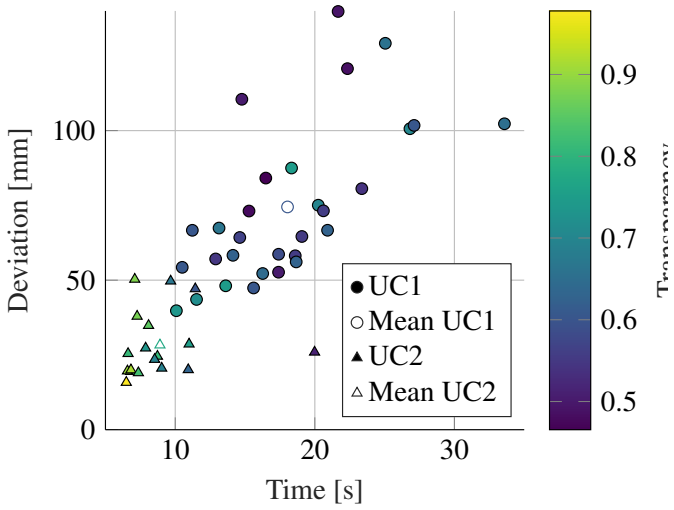

Figure 9: Participant performance comparison UC1/UC2, each circle is a UC1 participant and each triangle is a UC2 participant

Figure 10 shows the correlation of the performance criterion for both UCs using the *Matlab plotmatrix* and *corrcoeff* functions. Graphs on the diagonal and lower part of the matrix represent histogram and scatter plot of observation of mean performance for each participant in each UC. Values in the graphs on the upper part of the matrix indicate the linear correlation coefficients R between variables in rows and columns. The p-value of the coefficients is used to determine if the correlation is statistically significant (probability of the null hypothesis). Their corresponding significance is denoted with ** when the p-value is inferior to 0.01, * when the p-value is between 0.01 and 0.05 and n.s. when the p-value is superior to 0.05. A correlation coefficient which value is close to 1 or -1 indicates a strong dependence and 0 indicates independence. It can be noted that the *Time* and *Deviation* criterion have a significant correlation coefficient of 0.65 in the UC1 indicating that when participant have a good performance in term of *Time* they also have a good performance in term of *Deviation*. In the UC2, the variables *Time* and *Transparency* are also significantly correlated in the UC2 with a correlation coefficient of -0.81. This indicates that when the *Time* performance is good, the transparency performance is lower.

5.3. Comparing the training effect of UCs

Analysing the overall performance of the UCs presents the mean of performance but cannot define if the performance is affected by a training effect, that is to say if the performances of participants vary with the time of use of the system. To determine the training effect on the performance and the interaction quality the variations of the criteria with time of use of the system is analysed. The correlation between the performance criteria and PerformedPath is studied. A significant correlation between the number of PerformedPath and the performance criteria would indicate that the users of the system improve themselves using the system. In this section, the overall training effect is under study. Using all the performed paths of each

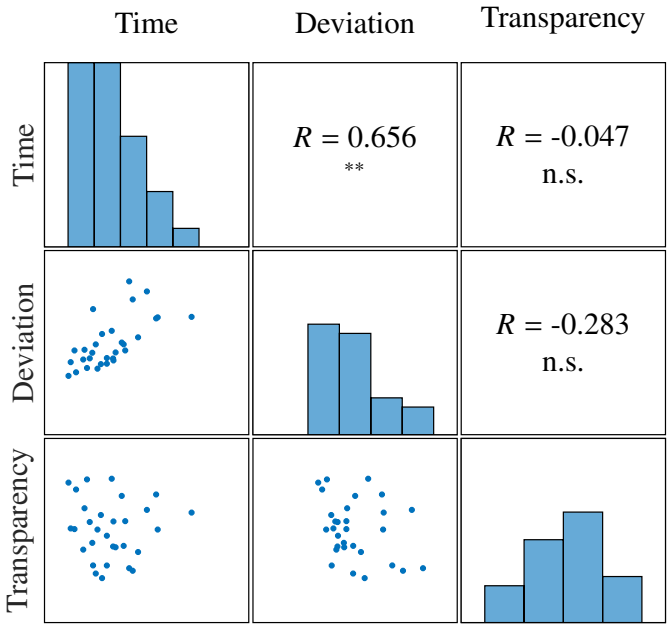

(a) Use Case 1

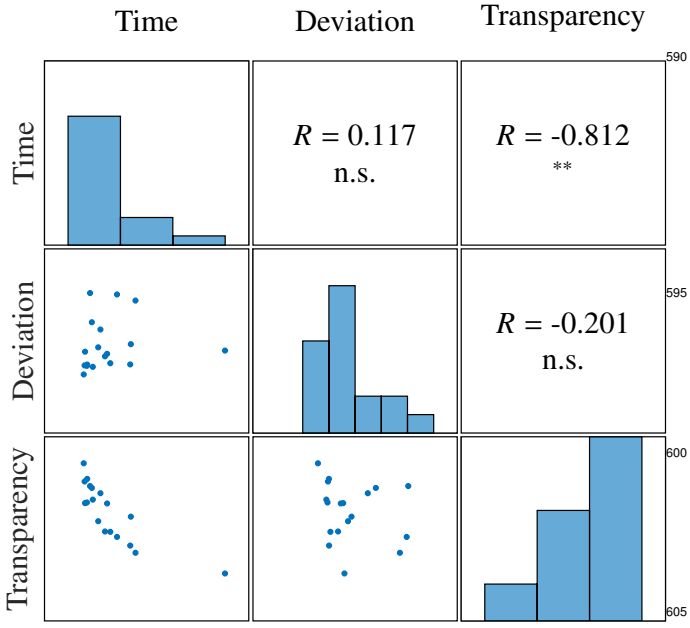

(b) Use Case 2

Figure 10: Correlation of performance criteria for both Use Cases, R is the linear correlation coefficient, ** denotes a p-value inferior to 0.01, * denotes a p-value between 0.01 and 0.05 and n.s. indicates a p-value superior to 0.05

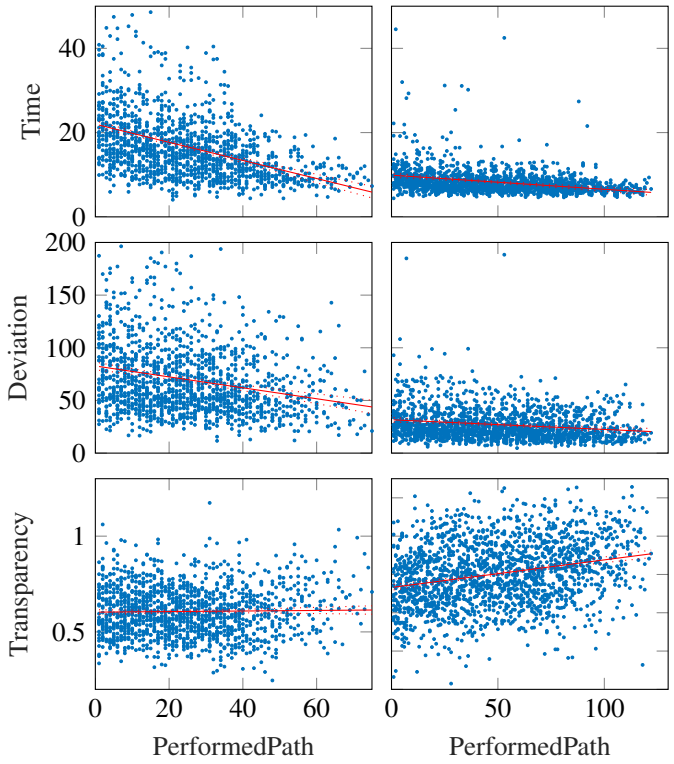

Figure 11: Plot of linear regression of all observations of performance criteria for each UC, blue scatter data are the observed segment and solid red line plot are linear model

UC, a linear regression model is fitted to each criterion for each participant so that:

$$y = a_0 + a_1 \text{PerformedPath} \tag{32}$$

where y is the response *Time*, *Deviation* or *Transparency*, a_0 and a_1 are the linear correlation coefficient. The p-value of the models are computed to determine whether each model is statistically more significant than a constant model. When the p-value is inferior to the defined α level ($\alpha = 0.05$ in this study) the constant model cannot be strongly rejected. For each response, 1362 observations (paths of 30 participants) for UC1 and 1517 observations (paths of 19 participants) for UC2 were analysed. Figure 11 plots the three performance criteria (*Time*, *Deviation* and *Transparency*) for every observed path of each user on separate UCs in blue. The fitted linear model line is plotted in red. The fitted coefficients obtained are shown in Table 3.

Considering the *Time* and *Deviation* performance criteria, fitted coefficients a_1 indicates a stronger progression in the UC1 while coefficients a_0 denote a better initial performance in the UC2. In term of *Transparency*, the fitted model for the UC1 is not statistically significant meaning that a linear correlation between the *Transparency* and the PerformedPath is not more probable than a constant model of *Transparency*.

5.4. Individually comparing performance variation

Analysing the overall variation of performance along PerformedPath for all participant denoted that the task performance

Table 3: Linear regression coefficients of performance criteria for each UC, ** denotes a p-value inferior to 0.01, * denotes a p-value between 0.01 and 0.05 and n.s. indicates a p-value superior to 0.05

		UC1	UC2
Time [s]	a_0	21.979	10.027
	a_1	-0.214 **	-0.033 **
Deviation [mm]	a_0	82	32
	a_1	-0.508 **	-0.087 **
Transparency [-]	a_0	0.602	0.715
	a_1	1.204e-04 n.s.	-1.005e-03 **

criteria (*Time* and *Deviation*) are overalls correlated with the PerformedPath. The *Transparency* for the UC1 however turned out to not be significantly correlated with PerformedPath. In addition, Figure 11 showed outliers that might have a different performance variation profile than the majority of users. For that reason, the individual variation of performance is studied for each participant. A linear regression is performed for each response of each participant of both UCs. The model defined in eq. 32 is fitted for all the observed paths of each participant. When the coefficients are statistically significant, the sign of a_1 is considered to classify the participants among three variation profiles namely regression, stagnation and progression. Table A.7 in Appendix A shows the fitted linear coefficients for the *Transparency* response of each participant that performed in the UC2. After assigning a performance variation profile to each participant, the occurrences of each profiles are counted.

To analyse the distribution of performance variation profiles of each performance metrics of both UC, two models are defined. M_h, described as homogenous model, corresponds to the hypothesis H_h supposing that the probability of each distribution is equal. M_t, as target model, corresponds to the hypothesis H_t supposing the two distribution have different probabilities. The likelihood of each model is computed and the ratio of L_t over L_h is $B_{t/h} = \frac{L_t}{L_h}$. If $B_{t/h}$ is less than 1, this indicates that the two distributions are not different and follow the same probability. A value superior to 1 denotes a different distribution probability therefore the two distributions are different.

Table 4 details the count of performance variation profiles for the *Time* in UC1 and UC2. For the *Time* criteria the ratio $B_{t/h} = 0.053$ denoting that the two distributions are not different. Both UCs have a higher proportion of participant stagnating and progressing than regressing on the *Time* performance.

Table 5 summarizes the count of the profiles for the *Deviation* in both UCs. The ratio for *Deviation* is $B_{t/h} = 0.137$ which tells that profile distribution is the same for both UCs. UC1 and UC2 have the same proportion of profiles. It can be seen that most participants progress and stagnate and few participant regress.

Table 6 details the count of performance variation profiles of the *Transparency* for both UCs. For the *Transparency*, the ratio $B_{t/h}$ is 2.077. In this case, the performance profile distribution of UC1 is different than the UC2. This indicates that the UC2 tends to have a higher proportion of participant regressing in term of *Transparency*.

Table 4: *Time* variation profiles distribution

		Regression	Stagnation	Progression
UC1	Proportions	0 %	46.7 %	53.3 %
	Counts	0	14	16
UC2	Proportions	0 %	52.6 %	47.4 %
	Counts	0	9	10
Total	Proportions	0 %	47.0 %	53.0 %
	Counts	0	23	26

Table 5: *Deviation* variation profiles distribution

		Regression	Stagnation	Progression
UC1	Proportions	6.7 %	60 %	33.3 %
	Counts	2	18	10
UC2	Proportions	0 %	63.1 %	36.9 %
	Counts	0	12	7
Total	Proportions	4.0 %	61.3 %	34.7 %
	Counts	2	30	17

6. Discussion

In this paper an experiment including a Collaborative Cable-Driven Parallel Robot was led involving human participants in the completion of a task. Two different robot configurations are compared. The first configuration includes a CDPR with three cables in a suspended configuration with a teleoperation working mode. The second configuration includes a CDPR with eight cables in a suspended configuration with a co-manipulation working mode. The control strategy and the task are common to the two Use Cases. Performance criteria were defined to assess the task completion quality as well as the interaction quality. The performances of both UCs were analysed and compared in order to assess the impact of the robot configuration and the nature of the interaction.

The nature of the task carried out was found to not have a significant effect on the performances in both UC. The time metric accounts for the differences in the path lengths and the metric of the deviation is not influenced by the length and the relative positions of the targets.

Table 6: *Transparency* variation profiles distribution

		Regression	Stagnation	Progression
UC1	Proportions	16.7 %	50 %	33.3 %
	Counts	5	15	10
UC2	Proportions	42.1 %	47.4 %	10.5 %
	Counts	8	9	2
Total	Proportions	26.5 %	49.0 %	24.5 %
	Counts	13	24	12

Overall performance analysis shows that the UC2 yields better task performances than the UC1. The performance improvement is associated to the nature of the interaction as participant of UC2 benefits from a better viewpoint of the task as they are closer to the targets. In addition the kinaesthetic sense is improved as they can feel better the robot motion. In UC1 the handle is fixed therefore no motion or force feedback of the robot is given to the participant. The transparency is found to be overalls better in UC1. This results arise from the nature of the movement executed by the participants. In UC1, participants tends to exert short force bursts onto the handle leading to the robot translation in the direction sought by the participant. Then the robot decelerates and stops and the participants exert another force in a different direction. In this case the robot is mostly decelerated by the dissipative term in the admittance control strategy. In the UC2, participants tend to have a continuous contact with the handle both for accelerating the MP in the desired direction and for decelerating when arriving close to the target. As the transparency varies when the participant is opposed to the robot motion, participants intrinsically spent more time opposing the robot motion in UC2 than in UC1.

Overall variations of performance metrics along time of use of the robot during experiment denote a training effect. Completion time and deviation performance increase faster in the UC1 but initial performance is better in UC2 therefore participants tend to progress slower in UC2 but have better performance. In term of transparency, the UC1 does not have one significant linear model overalls. This denote the presence of different variation profiles among the participant population. In UC2 the transparency tends to deteriorate overalls. The presence of outliers and less significant models for the whole participant population indicates the presence of different variation profiles.

Different variation profiles were identified among the participants. Regression, stagnation and progression profiles were defined based on the coefficients and significance of linear regression models for every participants. The UC1 have a higher proportion of participants improving the transparency than the UC2. This is explained by the fact that the training effect lead to longer and more accurate force bursts exerted by the participant to reach the targets. As the participants progress in time to complete the paths and in the deviation, they spent more time acting on the handle in the right direction and less time waiting for the robot to stop. Therefore, the transparency increased. A large proportion of participant have a decreasing transparency in UC2. This comes from the training effect and the task performance improvement. As they handle the robot, they tend to exert more force and increase the speed, therefore, the time spent decelerating the robot to not overshoot the target increase and lead to a decrease of the transparency.

7. Conclusion

In the scope of this paper, it was shown that the nature of the physical interaction between a human operator and a cable-driven parallel robot has a significant effect on the performance variation profiles among human users of a human-robot team. Teleoperation and co-manipulation modes impact differently the quality of the interaction evaluated using the defined transparency index. A collaborative robot should maximize the number of its users improving in term of task performance while being suited to account for the individuality of potential users. To do so, it is possible to consider using an adaptative control strategy for which the parameters vary to account for human variety of profiles. The parameter variation law can be based on the task performance metrics if available or on the interaction quality index. Such strategy can be found in the field of variable impedance control [30, 31]. Another perspective is to consider giving an information feedback to the user. The feedback could rely on the task completion metrics, if available, to let the user know on the performance of the human-robot team. This information might help the users to adapt their behaviour to improve the performance. In term of control theory this can be seen as an additional feedback loop where the robot controls the human [32].

Acknowledgment

This work was supported by the ANR CRAFT project, grant ANR-18-CE10-0004, https://anr.fr/Project-ANR-18-CE10-0004. The experimental protocol described in this paper has been approved by CERNI (the Nantes university ethical committee) on 17/07/2020. The research work was motivated by the EquipEx+ TIRREX project, grant ANR-21-ESRE-0015, too.

References

[1] Andreas Pott. *Cable-Driven Parallel Robots*, volume 120. Springer International Publishing, Cham, 2018.

[2] S. Kawamura, W. Choe, S. Tanaka, and S. R. Pandian. Development of an ultrahigh speed robot falcon using wire drive system. In *Proceedings of 1995 IEEE International Conference on Robotics and Automation*, pages 215–220. IEEE, 1995.

[3] Hui Li, Xinyu Zhang, Rui Yao, Jinghai Sun, Gaofeng Pan, and Wenbai Zhu. Optimal force distribution based on slack rope model in the incompletely constrained cable-driven parallel mechanism of fast telescope. In Tobias. Bruckmann and Andreas. Pott, editors, *Cable-driven parallel robots*, volume 12 of *Mechanisms and Machine Science*, pages 87–102. Springer-Verlag, Berlin and Heidelberg, 2013.

[4] Etienne Picard, Stéphane Caro, Franck Plestan, and Fabien Claveau. Control solution for a cable-driven parallel robot with highly variable payload. In *Volume 5B: 42nd Mechanisms and Robotics Conference*. American Society of Mechanical Engineers, 2018.

[5] Etienne Picard, Franck Plestan, Elias Tahoumi, Fabien Claveau, and Stéphane Caro. Control Strategies for a Cable-Driven Parallel Robot with Varying Payload Information. *Mechatronics*, 79:102648, November 2021.

[6] L. Gagliardini, S. Caro, M. Gouttefarde, and A. Girin. Discrete reconfiguration planning for cable-driven parallel robots. *Mechanism and Machine Theory*, 100:313–337, 2016.

[7] Antoine Martin, Stéphane Caro, and Philippe Cardou. Design of a cable-driven parallel robot with grasping device. *Procedia CIRP*, 70:290–295, 2018.

[8] Jean-Baptiste Izard, Alexandre Dubor, Pierre-Elie Hervé, Edouard Cabay, David Culla, Mariola Rodriguez, and Mikel Barrado. On the improvements of a cable-driven parallel robot for achieving additive manufacturing for construction. In Clément Gosselin, Philippe Cardou, Tobias Bruckmann, and Andreas Pott, editors, *Cable-Driven Parallel Robots*, volume 53 of *Mechanisms and Machine Science*, pages 353–363. Springer International Publishing, Cham, 2018.

[9] Alessandro Berti, Marco Carricato, and Marc Gouttefarde. Dynamic recovery of cable-suspended parallel robots after a cable failure. In Jadran Lenarčič and Jean-Pierre Merlet, editors, *Advances in Robot Kinematics 2016*, Springer Proceedings in Advanced Robotics. Springer International Publishing, Cham, 2018.

[10] Stéphane Caro and Jean-Pierre Merlet. Failure analysis of a collaborative 4-1 cable-driven parallel robot. In Doina Pisla, Burkhard Corves, and Calin Vaida, editors, *New Trends in Mechanism and Machine Science*, volume 89 of *Mechanisms and Machine Science*, pages 440–447. Springer, [S.l.], 2020.

[11] Guy Hoffman and Cynthia Breazeal. Collaboration in human-robot teams. In *AIAA 1st Intelligent Systems Technical Conference*, Reston, Virigina, 2004. American Institute of Aeronautics and Astronautics.

[12] Sara Kiesler and Michael A. Goodrich. The science of human-robot interaction. *ACM Transactions on Human-Robot Interaction*, 7(1):1–3, 2018.

[13] Jamil Abou Saleh and Fakhreddine Karray. Towards generalized performance metrics for human-robot interaction. In *2010 International Conference on Autonomous and Intelligent Systems, AIS 2010*, pages 1–6. IEEE, 2010.

[14] Michel Franken, Sarthak Misra, and Stefano Stramigioli. Improved transparency in energy-based bilateral telemanipulation. *Mechatronics*, 22(1):45–54, 2012.

[15] Ozgur Baser, Hakan Gurocak, and E. Ilhan Konukseven. Hybrid control algorithm to improve both stable impedance range and transparency in haptic devices. *Mechatronics*, 23(1):121–134, 2013.

[16] Daniel Budolak and Pinhas Ben-Tzvi. Series elastic actuation for improved transparency in time delayed haptic teleoperation. *Mechatronics*, 63:102278, 2019.

[17] Ilana Nisky, Ferdinando A. Mussa-Ivaldi, and Amir Karniel. Analytical study of perceptual and motor transparency in bilateral teleoperation. *IEEE Transactions on Human-Machine Systems*, 43(6):570–582, 2013.

[18] Nathanael Jarrasse, Jamie Paik, Viviane Pasqui, and Guillaume Morel. How can human motion prediction increase transparency? In *Robotics and Automation, 2008, ICRA 2008, IEEE International Conference on*, pages 2134–2139, [Pitscataway, NJ], 2008. IEEE Xplore.

[19] Kyeong Ha Lee, Seung Guk Baek, Hyuk Jin Lee, Hyouk Ryeol Choi, Hyungpil Moon, and Ja Choon Koo. Enhanced transparency for physical human-robot interaction using human hand impedance compensation. *IEEE/ASME Transactions on Mechatronics*, 23(6):2662–2670, 2018.

[20] Neil R. Carlson, William Buskist, C. Donald Heth, and Rod Schmaltz. *Psychology: The Science of Behaviour, Fourth Canadian Edition with MyPsychLab*. Pearson Education Canada, 2009.

[21] J. M. Hoc and R. Amalberti. Cognitive control dynamics for reaching a satisficing performance in complex dynamic situations. *Journal of Cognitive Engineering and Decision Making*, 1(1):22–55, 2007.

[22] Paul B. Baltes, Ursula M. Staudinger, and Ulman Lindenberger. Lifespan psychology: Theory and application to intellectual functioning. *Annual Review of Psychology*, 50(1):471–507, 1999.

[23] Guy Hoffman and Xuan Zhao. A primer for conducting experiments in human–robot interaction. *ACM Transactions on Human-Robot Interaction*, 10(1):1–31, 2021.

[24] Jeremy A. Marvel, Shelly Bagchi, Megan Zimmerman, and Brian Antonishek. Towards effective interface designs for collaborative hri in manufacturing. *ACM Transactions on Human-Robot Interaction*, 9(4):1–55, 2020.

[25] George Adamides, Georgios Christou, Christos Katsanos, Michalis Xenos, and Thanasis Hadzilacos. Usability guidelines for the design of robot teleoperation: A taxonomy. *IEEE Transactions on Human-Machine Systems*, 45(2):256–262, 2015.

[26] Caroline E. Harriott, Glenna L. Buford, Julie A. Adams, and Tao Zhang. Mental workload and task performance in peer-based human-robot teams. *ACM Transactions on Human-Robot Interaction*, 4(2):61–96, 2015.

[27] Jean Piaget. *The construction of reality in the child*, volume 20 of *International library of psychology : developmental psychology*. Routledge, Oxon [England], 1954.

[28] Lorenzo Gagliardini, Marc Gouttefarde, and Stephane Caro. Determination of a dynamic feasible workspace for cable-driven parallel robots. In Jadran Lenarčič and Jean-Pierre Merlet, editors, *Advances in Robot Kinematics 2016*, volume 4 of *Springer Proceedings in Advanced Robotics*, pages 361–370. Springer International Publishing, Cham, 2018.

[29] Philippe Lemoine, Pierre-Philippe Robet, Damien Chablat, Yannick Aoustin, and Maxime Gautier. Haptic control of the parallel robot orthoglide. In *24ème Congrès Français de Mécanique*, Brest, France, 2019.

[30] Fares J. Abu-Dakka and Matteo Saveriano. Variable impedance control and learning-a review. *Frontiers in robotics and AI*, 7:590681, 2020.

[31] Peng Song, Yueqing Yu, and Xuping Zhang. A tutorial survey and comparison of impedance control on robotic manipulation. *Robotica*, 37(5):801–836, 2019.

[32] Richard J. Jagacinski and John M. Flach. *Control Theory for Humans*. CRC Press, 2003.

Appendix A. Coefficients for transparency linear regression of UC2

Table A.7: Linear regression coefficients for *Transparency* variation in UC2 per participant, ** denotes a p-value inferior to 0.01, * denotes a p-value between 0.01 and 0.05 and n.s. indicates a p-value superior to 0.05

Participant	a_0	a_1	Profile
1	0.593	-4.337e-03 *	Progression
2	0.779	6.389e-04 n.s.	Stagnation
3	0.711	1.115e-03 *	Regression
4	0.636	-1.795e-04 n.s.	Stagnation
5	0.664	4.828e-05 n.s.	Stagnation
6	0.770	-7.514e-04 n.s.	Stagnation
7	0.787	1.318e-03 *	Regression
8	0.819	1.101e-03 *	Regression
9	0.629	1.330e-03 **	Regression
10	0.750	1.348e-03 *	Regression
11	0.853	-7.331e-04 n.s.	Stagnation
12	0.951	4.330e-04 n.s.	Stagnation
13	0.764	-1.625e-03 *	Progression
14	0.550	2.395e-03 n.s.	Stagnation
15	0.797	1.422e-03 **	Regression
16	0.812	1.482e-03 **	Regression
17	0.875	6.495e-04 n.s.	Stagnation
18	0.769	9.907e-04 **	Regression
19	0.822	6.228e-04 n.s.	Stagnation